

A cyclic stress softening model for the Mullins effect

S. R. Rickaby, N. H. Scott

School of Mathematics, University of East Anglia, Norwich Research Park, Norwich NR4 7TJ, UK

Abstract

In this paper the inelastic features of stress relaxation, hysteresis and residual strain are combined with the Arruda-Boyce eight-chain model of elasticity, in order to develop a model that is capable of describing the Mullins effect for cyclic stress-softening of an incompressible hyperelastic material, in particular a carbon-filled rubber vulcanizate. We have been unable to identify in the literature any other model that takes into consideration all the above inelastic features of the cyclic stress-softening of carbon-filled rubber. Our model compares favourably with experimental data and gives a good description of stress-softening, hysteresis, stress relaxation, residual strain and creep of residual strain.

Keywords: Mullins effect, stress-softening, hysteresis, stress relaxation, residual strain, creep of residual strain.

MSC codes: 74B20 · 74D10 · 74L15

1. Introduction

When a rubber specimen is loaded from the virgin state and then unloaded back to this original state, the subsequent load required to produce the same deformation is smaller than that required during primary loading. This phenomenon is known as stress-softening and may be thought of as a decay of elastic stiffness. Stress-softening is particularly evident in specimens of filled rubber vulcanizates. The vulcanizing of rubber is an irreversible process in which the chemical structure of the rubber is changed in order to improve its elasticity and strength. During the vulcanization of rubber cross-links are introduced chemically linking the polymer chains together.

Figure 1 represents the idealized stress-softening behaviour of a rubber specimen under uniaxial tension. The process starts from an unstressed and unstrained virgin state at point P_0 and time t_0 . Subsequently, the stress/strain relation follows path A , the primary loading path, until point P_1 is reached at a time t_1 . At this point P_1 , unloading of the specimen begins immediately and the stress/strain relation of the rubber follows the new path B , which lies below A , returning to the unstressed and unstrained state at point P_0 . If the material is then reloaded the stress-strain relation follows path B again, rather than path A , up to point P_1 . If the rubber is now strained beyond point P_1 then path D is activated, a continuation of the original primary loading path. If subsequent unloading occurs from the point P_2 , the rubber retracts along a new path C to the unstressed state at P_0 . The shape of this second stress-strain cycle differs significantly

Email addresses: stephen.r.rickaby@gmail.com (S. R. Rickaby), n.scott@uea.ac.uk (N. H. Scott)

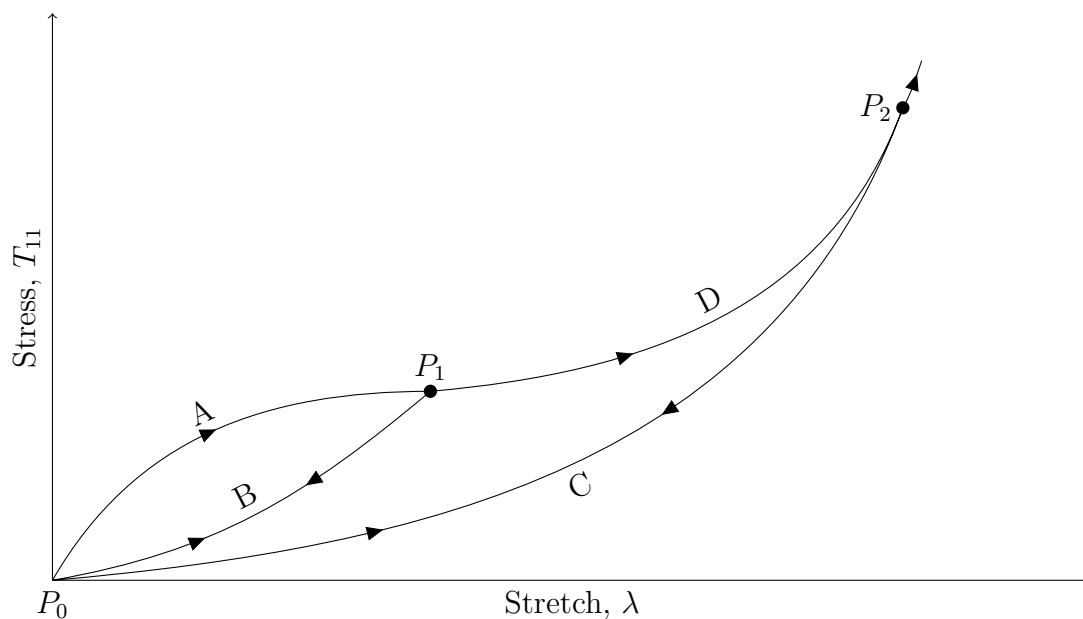


Figure 1: The idealized behaviour of stress-softening in rubber.

from the first. If the material is now reloaded the stress-strain behaviour follows the new path C , rejoining the primary loading path at the point P_2 .

This stress-softening phenomenon is known as the Mullins effect, named after Mullins who conducted an extensive study into carbon-filled rubber vulcanizates, see Mullins (1947). Diani et al. (2009) have written a recent review of this effect, detailing specific features associated with stress-softening and providing a précis of models developed to represent this effect.

Many authors have modelled the Mullins effect since Mullins, see, for example, Ogden and Roxburgh (1999), Dorfmann and Ogden (2004), Diani et al. (2009) and the references cited therein. However, most authors model a simplified version of the Mullins effect, in which the following inelastic features are neglected:

- Hysteresis
- Stress relaxation
- Residual strain
- Creep of residual strain

Despite the wealth of research into the Mullins effect over the last six or more decades we have been unable to identify in the literature any other model that has been used to reproduce the Mullins effect for cyclic stress-softening of unrefined experimental data.

For a typical carbon filled rubber vulcanizate it is evident from the experimental data presented in Figures 14, 15 and 16 that cyclically stretched carbon filled rubber vulcanizates undergo hysteresis, stress-relaxation, residual strain and creep of residual strain. Here, the unloading and reloading curves do not follow the same path and are positioned away from the origin with the successive relaxation paths being situated each below the previous one.

In this paper we derive an isotropic constitutive model to represent the Mullins effect for cyclic stress-softening under uniaxial tension. We explore the notion that in order to develop a

more realistic model of stress softening the above inelastic features must be included. However, not all softening features may be relevant for a particular application, and so in order to develop a functional model we require that specific parameters could be set to zero to exclude any particular inelastic feature above, and still maintain the integrity of the model.

The paper is constructed as follows. In Section 2 we describe the purely elastic response to the initial uniaxial tension in an incompressible isotropic non-linear elastic solid. We employ the elastic model of Arruda and Boyce (1993) but any other model of incompressible isotropic elasticity could be employed in its stead. In Section 3 we define the softening function which forms the basis of our new model for softening in uniaxial tension. Also in Section 3 we remodel the softening function of Dorfmann and Ogden (2003) to control the rate of softening and include the effects of hysteresis by defining separate softening functions for unloading and reloading. This is also a model for hysteresis, see Johnson and Beatty (1993). Section 4 models the effects of stress relaxation following the development of Bernstein et al. (1963) and Lockett (1972) and applies the model to cyclic stress relaxation. Section 5 presents a discussion of residual strain that is motivated by the work of Bergström and Boyce (1998) who develop a residual strain model by regarding it as a form of creep. In Section 6 we discuss the creep of residual strain and develop the Bergström and Boyce (1998) model to account for it. In Section 7 the models developed in Sections 2–6 are combined to obtain our new model for stress-softening of an incompressible isotropic elastic material in uniaxial tension which incorporates all the inelastic effects discussed in this paper. Finally, in Section 8 a graphical presentation of the model is provided and a comparison made between the model predictions and experimental data and conclusions are discussed in Section 9.

Preliminary results of the model were presented in Rickaby and Scott (2011).

2. Elastic response

In the reference configuration a material particle is located at position \mathbf{X} at time t_0 with Cartesian components X_1, X_2, X_3 . After deformation the same particle is located at the position $\mathbf{x}(\mathbf{X}, t)$, at time t , with Cartesian components x_1, x_2, x_3 . The deformation gradient is defined by

$$F_{iA}(\mathbf{X}, t) = \frac{\partial x_i(\mathbf{X}, t)}{\partial X_A}, \quad \text{or simply,} \quad \mathbf{F}(\mathbf{X}, t) = \frac{\partial \mathbf{x}(\mathbf{X}, t)}{\partial \mathbf{X}}.$$

An isochoric uniaxial strain is taken in the form

$$x_1 = \lambda X_1, \quad x_2 = \lambda^{-\frac{1}{2}} X_2, \quad x_3 = \lambda^{-\frac{1}{2}} X_3,$$

with λ denoting the uniaxial stretch. The left Cauchy-Green strain tensor $\mathbf{B} = \mathbf{F}\mathbf{F}^T$ is given by

$$\mathbf{B} = \begin{pmatrix} \lambda^2 & 0 & 0 \\ 0 & \lambda^{-1} & 0 \\ 0 & 0 & \lambda^{-1} \end{pmatrix},$$

with principal invariants

$$I_1 = \text{tr } \mathbf{B} = \lambda^2 + 2\lambda^{-1}, \quad I_2 = I_3 \text{tr } \mathbf{B}^{-1} = \lambda^{-2} + 2\lambda, \quad I_3 = 1, \quad (1)$$

the last following from isochoricity.

An incompressible isotropic hyperelastic material possesses a strain energy function $W(I_1, I_2)$ per unit volume in terms of which the Cauchy stress is given by

$$\mathbf{T}^{\mathcal{E}}(\lambda) = -p\mathbf{I} + 2 \left[\frac{\partial W}{\partial I_1} + I_1 \frac{\partial W}{\partial I_2} \right] \mathbf{B} - 2 \frac{\partial W}{\partial I_2} \mathbf{B}^2, \quad (2)$$

with p an arbitrary pressure and \mathbf{I} the unit tensor. We are concerned here only with uniaxial tension in the 1-direction and so may fix the value of p by the requirement

$$T_{22}^{\mathcal{E}}(\lambda) = T_{33}^{\mathcal{E}}(\lambda) = 0.$$

Using this value of p in equation (2) then gives the only non-zero component of stress to be the uniaxial tension

$$T_{11}^{\mathcal{E}}(\lambda) = 2(\lambda^2 - \lambda^{-1}) \left[\frac{\partial W}{\partial I_1} + \lambda^{-1} \frac{\partial W}{\partial I_2} \right], \quad (3)$$

in which equation (1)₁ has been used.

Equation (3) then gives the uniaxial stress $T_{11}^{\mathcal{E}}(\lambda)$ on the primary loading path A of Figure 1. Denote by λ_{\max} the value of the uniaxial stretch λ at the point P_1 on Figure 1. Along path A of Figure 1 we therefore have $1 \leq \lambda \leq \lambda_{\max}$.

2.1. The Arruda-Boyce eight-chain model

We now specialize to a particular model of incompressible non-linear isotropic elasticity both for definiteness and for comparison with experimental data in Section 8.2. We have selected the Arruda-Boyce eight-chain model as it requires only the measurement of two physical parameters. Furthermore, it has been shown to provide a good fit to experimental data, see Zúñiga and Beatty (2002). Rubber is composed of polymer chains, with each polymer chain being made-up of single links called monomers. This motivates the eight-chain model of Arruda and Boyce (1993) based upon the structure of a cube with eight polymer chains joining the corners of the cube to the central point. In the undeformed cube each such chain has the same length. If the deformation of the elastic material is such that the cube is deformed into a cuboid it remains true that all the chains have equal length, though in general a length different from that of the chain length associated with the original cube. Using this fact and arguments based on statistical mechanics Arruda and Boyce (1993) showed that the strain energy must take the form

$$W = \mu N \left\{ \left[\sqrt{\frac{I_1}{3N}} \right] \mathcal{L}^{-1} \left(\sqrt{\frac{I_1}{3N}} \right) + \log \left\{ \frac{\mathcal{L}^{-1} \left(\sqrt{\frac{I_1}{3N}} \right)}{\sinh \left(\mathcal{L}^{-1} \left(\sqrt{\frac{I_1}{3N}} \right) \right)} \right\} \right\} - h_0, \quad (4)$$

where μ is the positive ground state shear modulus, N is the number of links forming a single polymer chain and h_0 is a constant such that the strain energy vanishes in the undeformed state. $\mathcal{L}^{-1}(x)$ is the inverse function of the Langevin function

$$\mathcal{L}(x) = \coth x - \frac{1}{x}.$$

Upon substituting for W from equation (4) into equation (2) we obtain the stress in the Arruda-Boyce model:

$$\mathbf{T}^e(\lambda) = -p\mathbf{I} + \mu\sqrt{\frac{N}{3I_1}}\mathcal{L}^{-1}\left(\sqrt{\frac{I_1}{3N}}\right)\mathbf{B}, \quad (5)$$

and equation (3) for the single uniaxial stress reduces to

$$T_{11}^e(\lambda) = 2\mu(\lambda^2 - \lambda^{-1})\sqrt{\frac{N}{3I_1}}\mathcal{L}^{-1}\left(\sqrt{\frac{I_1}{3N}}\right). \quad (6)$$

3. Softening function and hysteresis

Zúñiga and Beatty (2002) defined the Cauchy stress \mathbf{T} in the unloading and reloading of the material to be a product of the Cauchy stress $\mathbf{T}^e(\lambda)$ in an isotropic elastic parent material, as in Section 2, and a softening function $\zeta(m)$ that depends on the current value of the magnitude of the strain m , where $m \equiv \sqrt{\mathbf{B} \cdot \mathbf{B}}$. However, in the present case of uniaxial tension it is more convenient to take as measure of strain magnitude simply the uniaxial strain λ , so that the softening function takes the form $\zeta(\lambda)$. We then have

$$\mathbf{T} = \zeta(\lambda)\mathbf{T}^e(\lambda) \quad (7)$$

along the unloading path B of Figure 1. At point P_1 the stresses on paths A and B must be equal and so equation (7) requires $\zeta(\lambda_{\max}) = 1$. Path B must be below path A and yet give positive stresses and so the function $\zeta(\lambda)$ must satisfy

$$0 < \zeta(\lambda) \leq 1 \quad \text{for} \quad 1 \leq \lambda \leq \lambda_{\max}, \quad (8)$$

with equality only for $\lambda = \lambda_{\max}$.

Dorfmann and Ogden (2003, 2004), employing a theory of pseudo-elasticity, effectively proposed as softening function

$$\zeta(\lambda) = 1 - \frac{1}{r}\tanh\left(\frac{W_{\max} - W}{\mu b}\right), \quad (9)$$

in which b and r are positive dimensionless material parameters. Choosing $r \geq 1$ ensures that $\zeta(\lambda) > 0$ for all choices of b . As before, μ is the ground state shear modulus. W_{\max} is the value which the strain energy W takes at the point P_1 . For stability it must be that the strain energy W is a monotonically increasing function of the uniaxial stretch λ . Since I_1 , defined by equation (1)₁, is a monotonically increasing function of λ in $\lambda \geq 1$, it follows that, for stability under uniaxial tension, W must be a monotonically increasing function of I_1 . Therefore $0 \leq W \leq W_{\max}$ on the primary loading path A . It follows that $\zeta(\lambda)$ defined by (9) satisfies the inequalities (8) and is monotonically increasing on $\lambda \geq 1$. It can be verified that the Arruda-Boyce strain energy function (4) is monotonically increasing on $\lambda \geq 1$.

(Johnson and Beatty, 1993, Section 3.6) observed that a typical stress-stretch response, that is obtained experimentally, is as depicted in Figure 2. Initial loading follows the path A up to

a point P_1 and subsequent unloading follows the path B , which lies below A . Reloading to the strain at P_1 then follows the new path C , which lies between A and B . Subsequent unloading from P_1 to P_0 and reloading from P_0 to P_1 follows paths B and C , respectively. The fact that path C lies above path B , and does not coincide with it, constitutes the phenomenon of hysteresis.

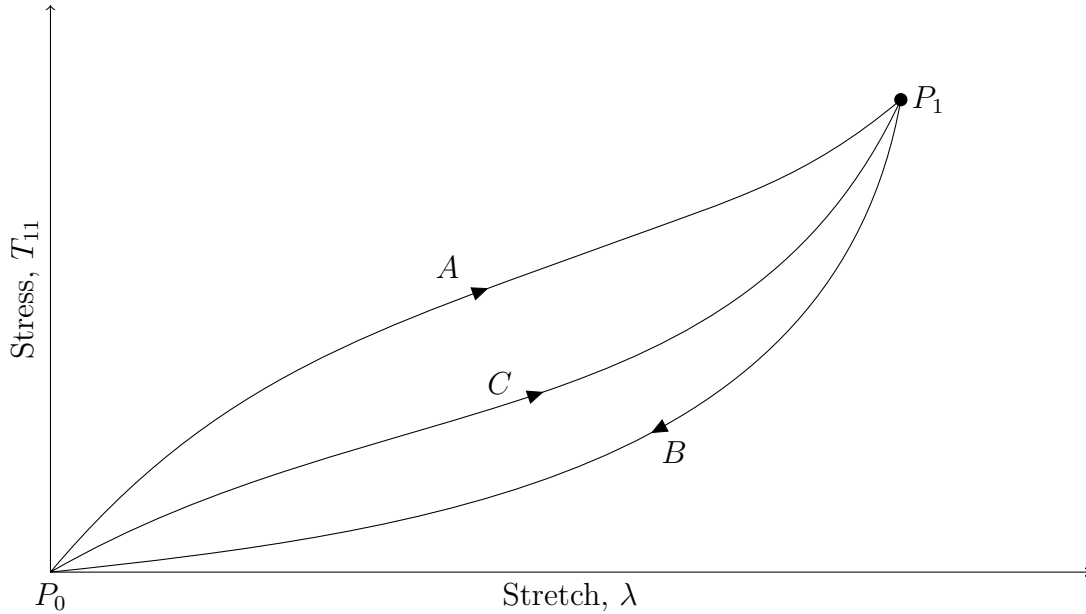


Figure 2: Stress-softening including hysteresis.

3.1. The softening functions for unloading and reloading

We shall model this unloading and reloading feature by introducing a dimensionless parameter ϑ_ω in order to control the rate at which the hyperbolic tangent term in equation (9) tends to zero as its argument tends to zero. We may then introduce a constant ϑ_1 for unloading and a different constant ϑ_2 for reloading. It turns out that we need also to give the parameters r and b in equation (9) different values in unloading and reloading. Therefore we shall replace the softening function of equation (9) by

$$\zeta_\omega(\lambda) = 1 - \frac{1}{r_\omega} \left\{ \tanh \left(\frac{W_{\max} - W}{\mu b_\omega} \right) \right\}^{1/\vartheta_\omega}, \quad (10)$$

where

$$\omega = \begin{cases} 1 & \text{unloading, following path } B, \\ 2 & \text{reloading, following path } C. \end{cases}$$

Choosing the parameters so that

$$r_2 \geq r_1 \geq 1, \quad b_2 \geq b_1, \quad \vartheta_2 \geq \vartheta_1,$$

with not all equalities holding together, guarantees that path C lies above path B , yet remains below path A , and that the inequalities (8) remain in force, taking here the form

$$0 < \zeta_1(\lambda) < \zeta_2(\lambda) < 1 \quad \text{for} \quad 1 \leq \lambda < \lambda_{\max},$$

with $\zeta_1(\lambda_{\max}) = \zeta_2(\lambda_{\max}) = 1$ continuing to hold.

On the primary loading path A of Figure 2 the elastic stress is given by $\mathbf{T}^e(\lambda)$, exactly as on the same path of Figure 1. Upon paths B and C of Figure 2 the stress is given by modifying (7) to read

$$\mathbf{T} = \zeta_\omega(\lambda)\mathbf{T}^e(\lambda), \quad (11)$$

where $\zeta_\omega(\lambda)$ is given by equation (10), with $\omega = 1$ corresponding to the unloading path B and $\omega = 2$ to the reloading path C .

When fitting this model to experimental data it is observed that as the stretch increases the stress relaxation paths underpredict the stress. By altering the softening parameter b , we can alter the curvature of the paths. This motivates assigning one softening parameter b_1 to the unloading path and a different softening parameter b_2 to the reloading path. The inclusion of the additional parameter ϑ_ω in the Dorfmann and Ogden (2003, 2004) model introduces further control of the shape of the softening function.

Equation (11) constitutes a model for hysteresis because it gives a reloading path C that is different from the unloading path B and lies above it. It does this by the introduction of a softening function (10) which is different on each of the paths B and C . This model is capable of representing the Mullins effect over multiple cycles of hysteresis and stress-softening. This approach has not previously been considered in the literature.

4. Cyclic stress relaxation

Suppose a material body is deformed in some way by applied stresses and is then held in the same state of deformation over a period of time by applied stress. Stress relaxation is said to occur if the stress needed to maintain this fixed deformation decreases over the period of time.

When a carbon filled rubber vulcanizate is cyclically loaded and unloaded to a specified strain, (Holt, 1931, Figure 1) observed that the successive relaxation paths are situated each below the previous one. This is illustrated in Figure 3, where the primary loading path P_0P_1 (i.e. path A) lies above the first reloading path P_0P_2 (i.e. path C) which, in turn, lies above the second reloading path P_0P_3 , and so on. Similarly, the first unloading path P_1P_0 (i.e. path B) lies above the second unloading path P_2P_0 , and so on. Eventually, equilibrium reloading and unloading paths are reached. Fletcher and Gent (1953) found experimentally that for rubber vulcanizates this viscoelastic stress relaxation is non-linear.

Dannenberg (1966) proposed that during primary loading of a vulcanized rubber, which is composed of polymer chains, some of the molecular cross-links or bonds between chains undergo slippage and breaking and that during subsequent stress relaxation some, but not all, of these broken bonds reform and the slippage partially recovers to its original position. In the present model we assume that the material does not relax during primary loading so that stress-relaxation occurs only during the subsequent unloading and reloading phases, commencing at time t_1 , the time at which primary loading ceased.

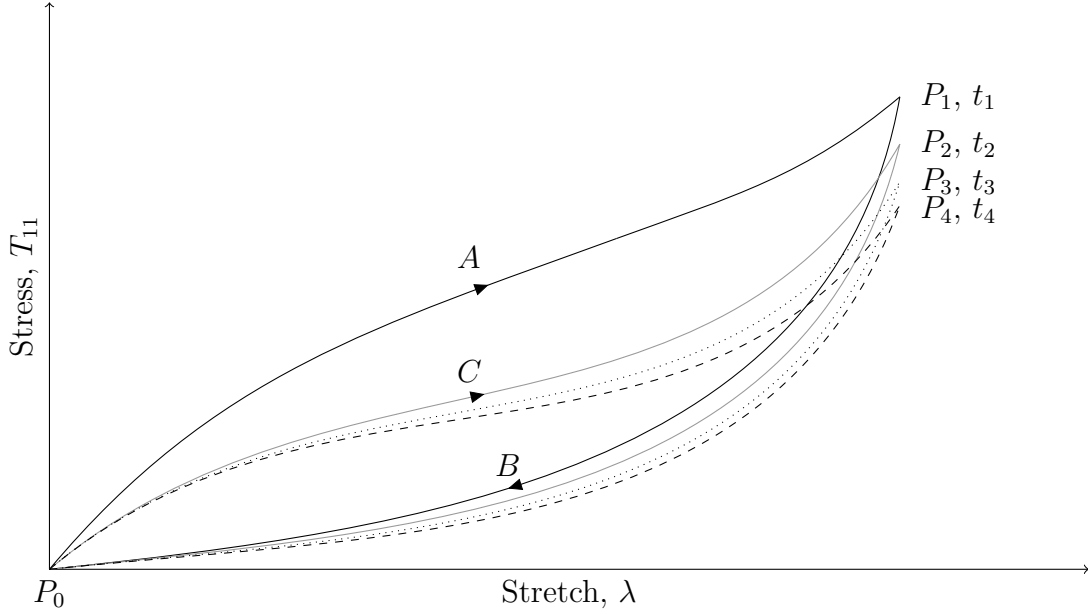


Figure 3: Cyclic stress relaxation.

Figure 3 represents a cyclically loaded and unloaded rubber specimen with primary loading occurring along path P_0P_1 up to the point P_1 where $\lambda = \lambda_{\max}$, which is reached at time t_1 . Stress-relaxation then commences at time t_1 and follows the unloading path P_1P_0 back to the position P_0 of zero stress, which is reached at time t_1^* . On the reloading path P_0P_2 stress-relaxation proceeds until point P_2 is reached, at time t_2 , where once again $\lambda = \lambda_{\max}$. Stress-relaxation continues as we follow the grey unloading path P_2P_0 to the position P_0 of zero stress, reached at time t_2^* . This pattern then continues throughout the unloading and reloading process. Stress-relaxation may proceed at different rates in unloading and reloading, i.e. $t_1^* - t_1$ and $t_2 - t_1^*$ may be unequal.

4.1. The Bernstein, Kearsley and Zapas model

Bernstein et al. (1963) developed a model, known as the BKZ model, for non-linear stress relaxation, postulating that if a material is observed at sufficiently low temperatures and for a short time, then it is difficult to distinguish its behaviour from that of an elastic solid. When the material is observed for a sufficiently long time and at a sufficiently high temperature, flow behaviour is more significant. The BKZ model has been found to represent accurately experimental data for stress-relaxation, see Tanner (1988) and the references therein.

For an incompressible viscoelastic solid, (Lockett, 1972, pages 114–116) derived the following version of the Bernstein et al. (1963) model for the relaxation stress $\mathbf{T}^{\mathcal{R}}$:

$$\mathbf{T}^{\mathcal{R}}(\lambda, t) = -p\mathbf{I} + \left[A_0 + \frac{1}{2}\check{A}_1(t)(I_1 - 3) - \check{A}_2(t) \right] \mathbf{B} + \check{A}_2(t)\mathbf{B}^2, \quad \text{for } t > t_1. \quad (12)$$

For uniaxial tension we argue as before to determine the pressure p from the requirement that $T_{22}^{\mathcal{R}} = T_{33}^{\mathcal{R}} = 0$ in equation (12), and then use this value of p to show that the only non-zero

component of stress in (12) is the uniaxial tension

$$T_{11}^{\mathcal{R}}(\lambda, t) = (\lambda^2 - \lambda^{-1}) \left[A_0 + \frac{1}{2} \check{A}_1(t) (\lambda - 1)^2 (1 + 2\lambda^{-1}) + \check{A}_2(t) (\lambda^2 - 1 + \lambda^{-1}) \right], \quad (13)$$

with $T_{11}^{\mathcal{R}}(\lambda, t)$ vanishing for $t \leq t_1$. In (12), A_0 is a material constant and $\check{A}_1(t)$, $\check{A}_2(t)$ are material functions which vanish for $t \leq t_1$ and are continuous for all t .

As a consequence of the above discussion for cyclic stress-relaxation the material functions $\check{A}_1(t)$ and $\check{A}_2(t)$ are replaced by

$$A_{1,2}(t) = \begin{cases} 0 & \text{primary loading, } t_0 \leq t \leq t_1, \text{ path } P_0P_1 \\ \check{A}_{1,2}(\phi_1(t - t_1)) & \text{unloading, } t_1 \leq t \leq t_1^*, \text{ path } P_1P_0 \\ \check{A}_{1,2}(\phi_2(t - t_1)) & \text{reloading, } t_1^* \leq t \leq t_2, \text{ path } P_0P_2 \\ \check{A}_{1,2}(\phi_1(t - t_1)) & \text{unloading, } t_2 \leq t \leq t_2^*, \text{ path } P_2P_0 \\ \check{A}_{1,2}(\phi_2(t - t_1)) & \text{reloading, } t_2^* \leq t \leq t_3, \text{ path } P_0P_3 \\ \dots & \dots \end{cases} \quad (14)$$

with ϕ_1 and ϕ_2 being continuous functions of time. Separate functions ϕ_1 and ϕ_2 are needed for the unloading and reloading phases, respectively, in order to model better the experimental data in Section 8.2.

Employing equation (14), equation (13) becomes,

$$T_{11}^{\mathcal{R}}(\lambda, t) = (\lambda^2 - \lambda^{-1}) \left[A_0 + \frac{1}{2} A_1(t) (\lambda - 1)^2 (1 + 2\lambda^{-1}) + A_2(t) (\lambda^2 - 1 + \lambda^{-1}) \right]. \quad (15)$$

In Figure 4 we illustrate possible forms of $A_1(t)$ and $A_2(t)$.

4.2. The total Cauchy stress in stress relaxation

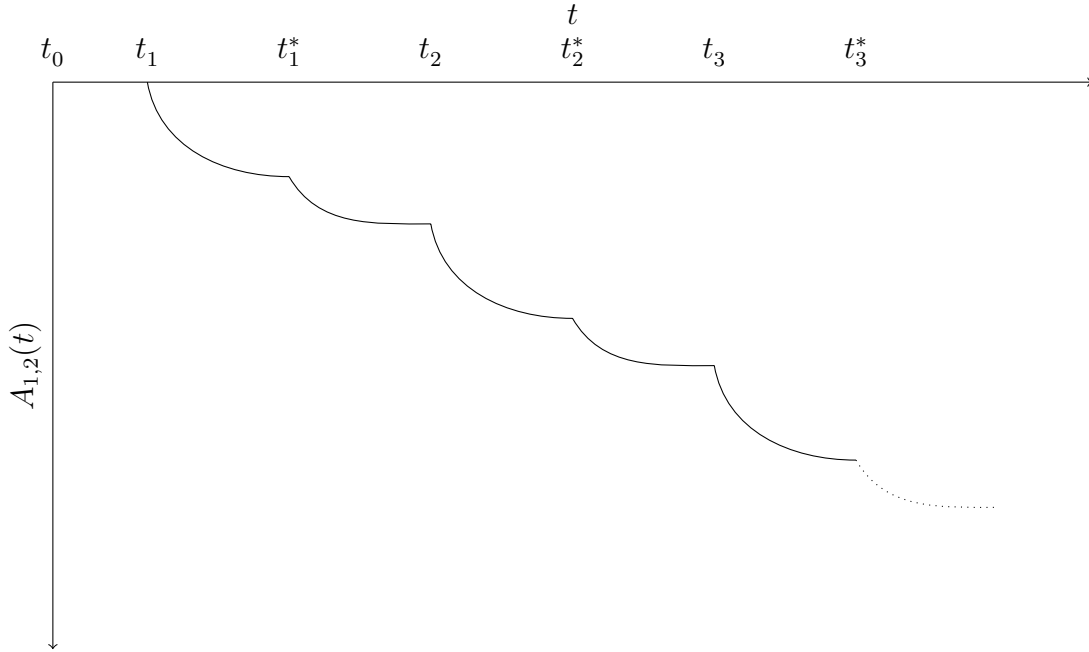
From the results of this section we see that the total Cauchy stress \mathbf{T} in a material which displays stress relaxation, softening and hysteresis is given by

$$\mathbf{T} = \begin{cases} \mathbf{T}^{\mathcal{E}}(\lambda), & \text{primary loading, } t_0 \leq t \leq t_1, \text{ path } P_0P_1 \\ \zeta_1(\lambda) \{ \mathbf{T}^{\mathcal{E}}(\lambda) + \mathbf{T}^{\mathcal{R}}(\lambda, t) \}, & \text{unloading, } t_1 \leq t \leq t_1^*, \text{ path } P_1P_0 \\ \zeta_2(\lambda) \{ \mathbf{T}^{\mathcal{E}}(\lambda) + \mathbf{T}^{\mathcal{R}}(\lambda, t) \}, & \text{reloading, } t_1^* \leq t \leq t_2, \text{ path } P_0P_2 \\ \zeta_1(\lambda) \{ \mathbf{T}^{\mathcal{E}}(\lambda) + \mathbf{T}^{\mathcal{R}}(\lambda, t) \}, & \text{unloading, } t_2 \leq t \leq t_2^*, \text{ path } P_2P_0 \\ \zeta_2(\lambda) \{ \mathbf{T}^{\mathcal{E}}(\lambda) + \mathbf{T}^{\mathcal{R}}(\lambda, t) \}, & \text{reloading, } t_2^* \leq t \leq t_3, \text{ path } P_0P_3 \\ \dots & \dots \end{cases} \quad (16)$$

where $\mathbf{T}^{\mathcal{E}}(\lambda)$ is the elastic stress (5) and $\mathbf{T}^{\mathcal{R}}(\lambda, t)$ is the relaxation stress (12).

The total stress (16) falls to zero in $t > t_1$ and so we must have $T_{11}^{\mathcal{R}} < 0$ for $t > t_1$, implying that $T_{11}^{\mathcal{R}} < 0$ for $\lambda > 1$. Each of the quantities A_0 , $A_1(t)$, $A_2(t)$ occurring in equation (15) has positive coefficient for $\lambda > 1$ and so at least one of them must be negative to maintain the requirement $T_{11}^{\mathcal{R}} < 0$ for $\lambda > 1$. In fact, we find in practice that all of them are negative.

Many authors have used the BKZ model and variations of it, though to our knowledge this is the first time it has been coupled with the Arruda-Boyce model to devise a model for stress-softening, hysteresis and stress relaxation.

Figure 4: Graphical representation of $A_{1,2}(t)$.

5. Residual strain

When a specimen of vulcanized rubber undergoes uniaxial tension it is observed that the unloading path might not return to the origin P_0 at zero stress but rather to a different point P_1^* , at strain $\lambda_1^* > 1$, as indicated by the diamond marker in Figure 5. The unloading path $P_1 P_1^*$ is shown as a dashed line in Figure 5. The distance between the point P_1^* , where the unloading path reaches zero stress, and the origin P_0 , i.e. $\lambda_1^* - 1$, is a measure of the increase in length of the material, that is, the degree of creep sustained by the material during unloading and reloading.

5.1. The creep model of Bergström and Boyce

Bergström and Boyce (1998) introduced a continuum model of effective creep in order to explain the existence of residual strain. Their model is based on the theoretical work of (Doi and Edwards, 1986, page 213) which itself is rooted in statistical mechanics. The length of a polymer chain is denoted by λ_{chain} and the Arruda and Boyce (1993) eight-chain model is employed once more to deduce that for an isotropic material

$$\lambda_{\text{chain}} = \sqrt{\frac{I_1}{3}}.$$

This equation has been used by (Bergström and Boyce, 1998, eqn 22 and 23) to derive the following equation which describes how the effective creep rate depends on the chain length, and so on the first invariant I_1 of \mathbf{B} :

$$\text{effective creep rate} = c [\lambda_{\text{chain}} - 1]^{-1} = c \left[\sqrt{\frac{I_1}{3}} - 1 \right]^{-1}, \quad (17)$$

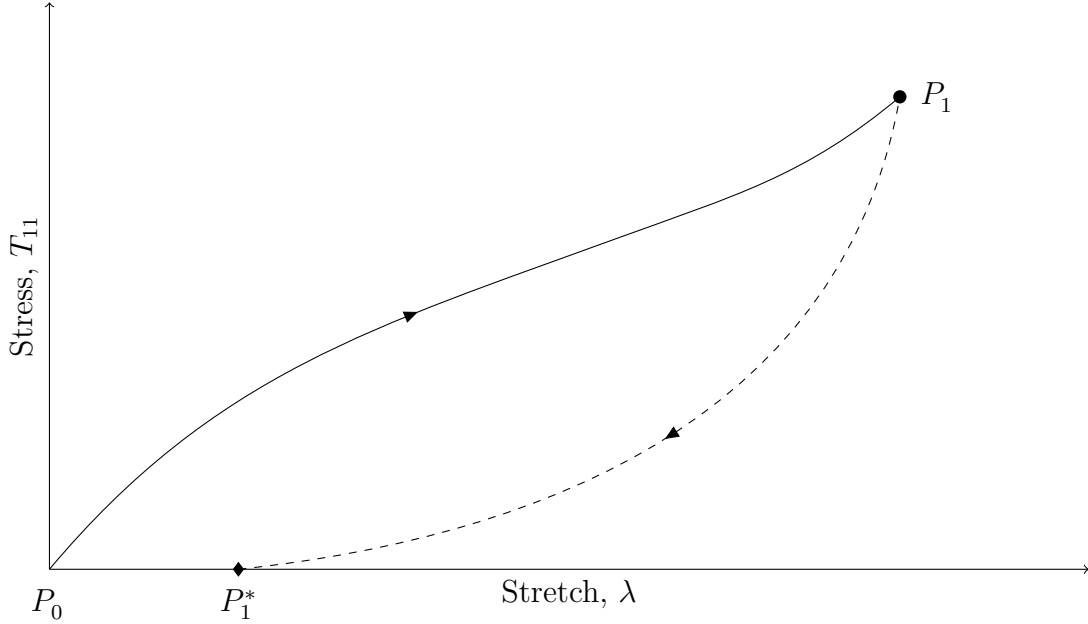


Figure 5: Residual strain in stress-softened rubber.

where c is a constant.

The time dependence of a cyclically stretched rubber specimen is illustrated in Figure 6. Initially, the specimen is loaded to the strain $\lambda = \lambda_{\max}$ at point P_1 and time t_1 . The material is then unloaded to zero stress at point P_1^* and time t_1^* , at which point the strain is $\lambda_1^* > 1$. Reloading commences immediately at time t_1^* , terminating at the strain $\lambda = \lambda_{\max}$ at point P_2 and time t_2 . The material is then unloaded to zero stress at point P_2^* and time t_2^* , at which point the strain is $\lambda_2^* > \lambda_1^* > 1$. Reloading then commences immediately at time t_2^* , and so on. The points P_n^* are indicated by the diamond markers in Figure 6. This pattern continues throughout the reloading and unloading process as the paths tend to equilibrium positions. Due to the inherent stress-softening features of the material the time intervals $t_1^* - t_1$ and $t_2^* - t_2$ may be unequal.

5.2. An extension of the model of Bergström and Boyce

To predict the amount of residual strain accruing during cyclic unloading and reloading we replace the constant c in equation (17) by a time dependent function $c(t)$ such as

$$c(t) = d[1 + [\tanh \check{a}(t)]^{a_1}], \quad (18)$$

where $a_1 > 0$ and d are material constants and $\check{a}(t) > 0$ is a continuous, increasing function of time. As $t \rightarrow \infty$ we see that $c(t) \rightarrow 2d$ so that the unloading and reloading paths tend to equilibrium values. This function is capable of representing experimental data for suitable choice of d , a_1 and $\check{a}(t)$. The constant d is selected to ensure that the first unloading path $P_1 P_1^*$ ceases at the point P_1^* .

We assume that creep leading to residual strain does not occur during primary loading but evolves throughout the unloading and reloading process, though this creep may run at different rates on the unloading and reloading paths.

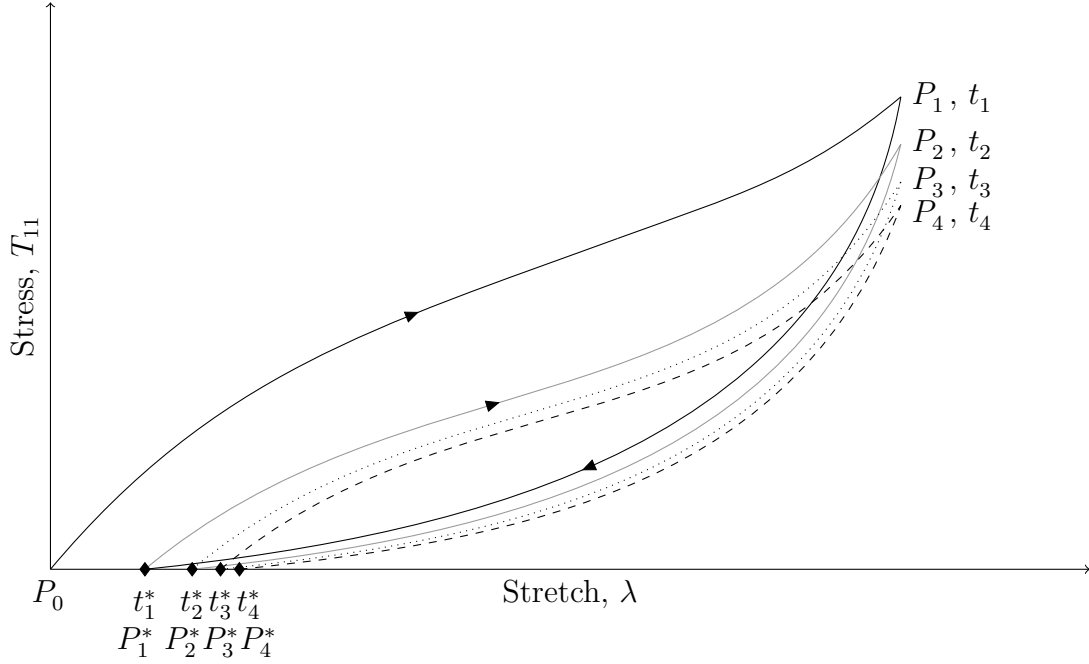


Figure 6: Cyclic stress-softening.

The function $a(t)$ is defined by

$$a(t) = \begin{cases} 0 & \text{primary loading, } t_0 \leq t \leq t_1, \text{ path } P_0 P_1 \\ \check{a}(\Phi_1(t - t_1)) & \text{unloading, } t_1 \leq t \leq t_1^*, \text{ path } P_1 P_1^* \\ \check{a}(\Phi_2(t - t_1)) & \text{reloading, } t_1^* \leq t \leq t_2, \text{ path } P_1^* P_2 \\ \check{a}(\Phi_1(t - t_1)) & \text{unloading, } t_2 \leq t \leq t_2^*, \text{ path } P_2 P_2^* \\ \check{a}(\Phi_2(t - t_1)) & \text{reloading, } t_2^* \leq t \leq t_3, \text{ path } P_2^* P_3 \\ \dots & \dots \end{cases} \quad (19)$$

with Φ_1 and Φ_2 being continuous functions of time. The form of $a(t)$ is similar to that of $A_{1,2}(t)$ shown in Figure 4.

In the current model it is assumed that the specimen of rubber is being cyclically stretched to the same final strain λ_{\max} . During each cycle the residual stretch λ_n^* of the unloaded specimen at point P_n^* increases until an equilibrium state is reached. By combining equations (17) and (18) we obtain an expression for the Cauchy stress when the material is undergoing a number of unloading and reloading cycles:

$$\mathbf{T}^{\mathcal{E}}(\lambda, t) = -p\mathbf{I} + \left\{ d \left[\sqrt{\frac{I_1}{3}} - 1 \right]^{-1} [1 + [\tanh a(t)]^{\alpha_1}] \right\} \mathbf{B} \quad \text{for } t > t_1 \text{ and } \lambda > 1. \quad (20)$$

The number of cycles is accounted for in equation (20) by the definition (19) of $a(t)$.

For $t < t_1$ and $\lambda = 1$, $\mathbf{T}^{\mathcal{E}}(\lambda, t)$ must vanish as there is no residual strain. The singularity of equation (20) at $\lambda = 1$ is not relevant as the residual strains all satisfy $\lambda_n^* > 1$.

From equation (20) applied to uniaxial tension, after eliminating p , we obtain

$$T_{11}^{\mathcal{C}}(\lambda, t) = d \left[\lambda^2 - \frac{1}{\lambda} \right] \left[\sqrt{\frac{I_1}{3}} - 1 \right]^{-1} [1 + [\tanh a(t)]^{a_1}]. \quad (21)$$

The total stress (21) falls to zero in $t > t_1^*$ and so we must have $T_{11}^{\mathcal{C}} < 0$ for $t > t_1^*$, implying that $T_{11}^{\mathcal{C}} < 0$ for $\lambda > 1$. This requirement forces $d < 0$ in equation (21).

It follows that the total Cauchy stress \mathbf{T} in a material displaying stress relaxation, softening, hysteresis and residual strain is given by

$$\mathbf{T} = \begin{cases} \mathbf{T}^{\mathcal{E}}(\lambda), & \text{primary loading, } t_0 \leq t \leq t_1, \text{ path } P_0 P_1 \\ \zeta_1(\lambda) \mathbf{T}^{\mathcal{E}+\mathcal{R}+\mathcal{C}}(\lambda, t), & \text{unloading, } t_1 \leq t \leq t_1^*, \text{ path } P_1 P_1^* \\ \zeta_2(\lambda) \mathbf{T}^{\mathcal{E}+\mathcal{R}+\mathcal{C}}(\lambda, t), & \text{reloading, } t_1^* \leq t \leq t_2, \text{ path } P_1^* P_2 \\ \zeta_1(\lambda) \mathbf{T}^{\mathcal{E}+\mathcal{R}+\mathcal{C}}(\lambda, t), & \text{unloading, } t_2 \leq t \leq t_2^*, \text{ path } P_2 P_2^* \\ \zeta_2(\lambda) \mathbf{T}^{\mathcal{E}+\mathcal{R}+\mathcal{C}}(\lambda, t), & \text{reloading, } t_2^* \leq t \leq t_3, \text{ path } P_2^* P_3 \\ \dots & \dots \quad \dots \quad \dots \end{cases} \quad (22)$$

in which for notational convenience we have defined a stress

$$\mathbf{T}^{\mathcal{E}+\mathcal{R}+\mathcal{C}}(\lambda, t) = \mathbf{T}^{\mathcal{E}}(\lambda) + \mathbf{T}^{\mathcal{R}}(\lambda, t) + \mathbf{T}^{\mathcal{C}}(\lambda, t), \quad (23)$$

where $\mathbf{T}^{\mathcal{E}}(\lambda)$, $\mathbf{T}^{\mathcal{R}}(\lambda, t)$ and $\mathbf{T}^{\mathcal{C}}(\lambda, t)$ are given by equations (5), (12) and (20), respectively.

6. Creep of residual strain

Suppose now that reloading does not commence at the same time t_n^* that unloading ceased, as was the case in Figure 6. Instead, the material that was fully unloaded at time t_n^* and stretch λ_n^* is now left stress free until the later time t_n^{**} when the point P_n^{**} is reached, with stretch λ_n^{**} , satisfying $1 < \lambda_n^{**} < \lambda_n^*$. Then at time t_n^{**} reloading recommences and proceeds until the point P_{n+1} is reached. This new phenomenon is illustrated in Figure 7 where diamond markers indicate where unloading ceases (as before) and square markers indicate the new points where reloading commences.

It is observed experimentally that during cyclic unloading and reloading the relaxation paths progressively move away from the first unloading and reloading paths until an equilibrium state is reached, as illustrated in Figure 7, and highlighted there by the diamond and square markers moving to the right as time progresses. Due to the inherent stress-softening features of the material the time intervals $t_1^* - t_1$ and $t_2^* - t_2$ may be unequal as also may $t_1^{**} - t_1$ and $t_2^{**} - t_2$.

The stress-relaxation functions $A_{1,2}(t)$ and residual strain function $a(t)$ operate during unloading and reloading and also for the time periods $t_n^* \leq t \leq t_n^{**}$ of zero stress. During these stress-free time periods the material continues to undergo stress relaxation. Thus equation (14)

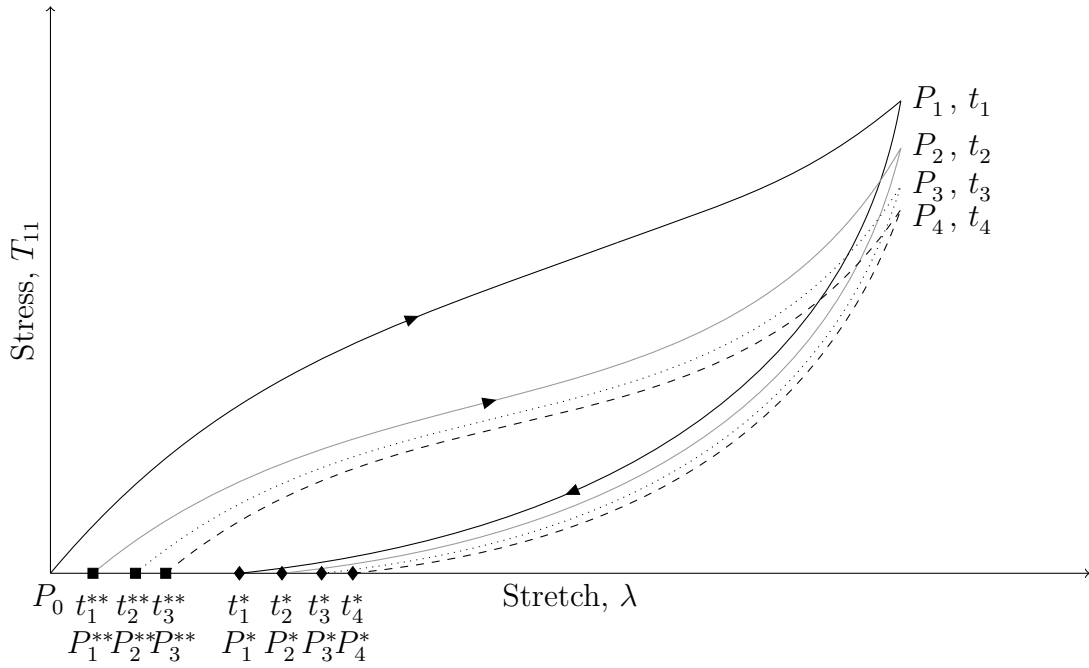


Figure 7: Cyclic stress-softening with residual strain.

is replaced by

$$A_{1,2}(t) = \begin{cases} 0 & \text{primary loading, } t_0 \leq t \leq t_1, & \text{path } P_0 P_1 \\ \check{A}_{1,2}(\phi_1(t - t_1)) & \text{unloading, } t_1 \leq t \leq t_1^*, & \text{path } P_1 P_1^* \\ \check{A}_{1,2}(\phi_1(t - t_1)) & \text{stress free, } t_1^* \leq t \leq t_1^{**}, & \text{path } P_1^* P_1^{**} \\ \check{A}_{1,2}(\phi_2(t - t_1)) & \text{reloading, } t_1^{**} \leq t \leq t_2, & \text{path } P_1^{**} P_2 \\ \check{A}_{1,2}(\phi_1(t - t_1)) & \text{unloading, } t_2 \leq t \leq t_2^*, & \text{path } P_2 P_2^* \\ \check{A}_{1,2}(\phi_1(t - t_1)) & \text{stress free, } t_2^* \leq t \leq t_2^{**}, & \text{path } P_2^* P_2^{**} \\ \check{A}_{1,2}(\phi_2(t - t_1)) & \text{reloading, } t_2^{**} \leq t \leq t_3, & \text{path } P_2^{**} P_3 \\ \dots & \dots & \dots \end{cases} \quad (24)$$

where ϕ_1 and ϕ_2 are as in (14). For simplicity, on the stress-free paths we employ ϕ_1 as the argument for $A_{1,2}(t)$ as we did on the unloading paths.

The residual strain function $a(t)$, defined by equation (19), is replaced by

$$a(t) = \begin{cases} 0 & \text{primary loading, } t_0 \leq t \leq t_1, & \text{path } P_0 P_1 \\ \check{a}(\Phi_1(t - t_1)) & \text{unloading, } t_1 \leq t \leq t_1^*, & \text{path } P_1 P_1^* \\ \check{a}(\Phi_1(t - t_1)) & \text{stress free, } t_1^* \leq t \leq t_1^{**}, & \text{path } P_1^* P_1^{**} \\ \check{a}(\Phi_2(t - t_1)) & \text{reloading, } t_1^{**} \leq t \leq t_2, & \text{path } P_1^{**} P_2 \\ \check{a}(\Phi_1(t - t_1)) & \text{unloading, } t_2 \leq t \leq t_2^*, & \text{path } P_2 P_2^* \\ \check{a}(\Phi_1(t - t_1)) & \text{stress free, } t_2^* \leq t \leq t_2^{**}, & \text{path } P_2^* P_2^{**} \\ \check{a}(\Phi_2(t - t_1)) & \text{reloading, } t_2^{**} \leq t \leq t_3, & \text{path } P_2^{**} P_3 \\ \dots & \dots & \dots \end{cases} \quad (25)$$

where Φ_1 and Φ_2 are as in equation (19). For simplicity, on the stress-free paths we employ Φ_1 as the argument for $a(t)$ as we did on the unloading paths.

In order to account for any change in residual strain during the time periods $t_n^* \leq t \leq t_n^{**}$, the stress-free range in equation (25), we replace the constant d in equation (21) by d_ω , allowing it to take a value d_1 for unloading and a different value d_2 for reloading. Then equation (20) becomes

$$\mathbf{T}^\mathcal{E}(\lambda, t) = -p\mathbf{I} + \left\{ d_\omega \left[\sqrt{\frac{I_1}{3}} - 1 \right]^{-1} [1 + [\tanh a(t)]^{a_1}] \right\} \mathbf{B} \quad \text{for } t > t_1 \text{ and } \lambda > 1, \quad (26)$$

and the corresponding uniaxial stress $T_{11}^\mathcal{E}(\lambda, t)$ is given by equation (21) with d replaced by d_ω .

7. Constitutive model

From the results of the previous section it follows that the total Cauchy stress \mathbf{T} in a material displaying softening, hysteresis, stress relaxation, residual strain and creep of residual strain is given by

$$\mathbf{T} = \begin{cases} \mathbf{T}^\mathcal{E}(\lambda), & \text{primary loading, } t_0 \leq t \leq t_1, & \text{path } P_0 P_1 \\ \zeta_1(\lambda) \mathbf{T}^{\mathcal{E}+\mathcal{R}+\mathcal{C}}(\lambda, t), & \text{unloading, } t_1 \leq t \leq t_1^*, & \text{path } P_1 P_1^* \\ \mathbf{0}, & \text{stress free, } t_1^* \leq t \leq t_1^{**}, & \text{path } P_1^* P_1^{**} \\ \zeta_2(\lambda) \mathbf{T}^{\mathcal{E}+\mathcal{R}+\mathcal{C}}(\lambda, t), & \text{reloading, } t_1^{**} \leq t \leq t_2, & \text{path } P_1^{**} P_2 \\ \zeta_1(\lambda) \mathbf{T}^{\mathcal{E}+\mathcal{R}+\mathcal{C}}(\lambda, t), & \text{unloading, } t_2 \leq t \leq t_2^*, & \text{path } P_2 P_2^* \\ \mathbf{0}, & \text{stress free, } t_2^* \leq t \leq t_2^{**}, & \text{path } P_2^* P_2^{**} \\ \zeta_2(\lambda) \mathbf{T}^{\mathcal{E}+\mathcal{R}+\mathcal{C}}(\lambda, t), & \text{reloading, } t_2^{**} \leq t \leq t_3, & \text{path } P_2^{**} P_3 \\ \dots & \dots & \dots \end{cases} \quad (27)$$

where once again the stress $\mathbf{T}^{\mathcal{E}+\mathcal{R}+\mathcal{C}}(\lambda, t)$, defined by (23), is employed for notational convenience, except that here $\mathbf{T}^\mathcal{E}(\lambda, t)$ is given by equation (26) rather than by equation (20).

To the best of our knowledge the effects of residual strain in relation to the Mullins effect during cyclic loading have not previously been considered in the literature and so the resulting equation (27) for the stress has not previously been exhibited.

On substituting the individual stresses given by equations (6), (15) and (26) into equation (27), we obtain the following constitutive model for the Cauchy stress \mathbf{T} in an incompressible isotropic solid material that models stress-softening, hysteresis, stress relaxation, residual strain and creep of residual strain:

$$\begin{aligned} \mathbf{T} = & \left[1 - \frac{1}{r_\omega} \left\{ \tanh \left(\frac{W_{\max} - W}{\mu b_\omega} \right) \right\}^{1/\vartheta_\omega} \right] \times \\ & \times \left\{ -p\mathbf{I} + \mu \sqrt{\frac{N}{3I_1}} \mathcal{L}^{-1} \left(\sqrt{\frac{I_1}{3N}} \right) \mathbf{B} \right. \\ & + \left[A_0 \mathbf{B} + \frac{1}{2} A_1(t) (I_1 - 3) \mathbf{B} + A_2(t) (\mathbf{B}^2 - \mathbf{B}) \right] \\ & \left. + d_\omega \left[\sqrt{\frac{I_1}{3}} - 1 \right]^{-1} [1 + [\tanh a(t)]^{a_1}] \mathbf{B} \right\}. \end{aligned} \quad (28)$$

As before, we eliminate p from equation (28) to obtain the uniaxial tension

$$\begin{aligned} T_{11} = & \left[1 - \frac{1}{r_\omega} \left\{ \tanh \left(\frac{W_{\max} - W}{\mu b_\omega} \right) \right\}^{1/\vartheta_\omega} \right] \times \\ & \times \left\{ \mu (\lambda^2 - \lambda^{-1}) \sqrt{\frac{N}{3I_1}} \mathcal{L}^{-1} \left(\sqrt{\frac{I_1}{3N}} \right) \right. \\ & + (\lambda^2 - \lambda^{-1}) \left[A_0 + \frac{1}{2} A_1(t) (\lambda - 1)^2 (1 + 2\lambda^{-1}) + A_2(t) (\lambda^2 - 1 + \lambda^{-1}) \right] \\ & \left. + d_\omega (\lambda^2 - \lambda^{-1}) \left[\sqrt{\frac{I_1}{3}} - 1 \right]^{-1} [1 + [\tanh a(t)]^{a_1}] \right\}. \end{aligned} \quad (29)$$

The authors believe that this constitutive equation for cyclic stress-softening in the Mullins effect is the first to incorporate all the inelastic effects of hysteresis, stress-relaxation, residual strain and creep of residual strain.

8. Numerical examples and comparison with experimental data

In our numerical work we approximate the inverse Langevin function by its Padé approximant derived by Cohen (1991), namely,

$$\mathcal{L}^{-1}(x) \approx \frac{3x - x^3}{1 - x^2}. \quad (30)$$

Figure 8 illustrates the close agreement between the inverse Langevin function and its approximation (30).

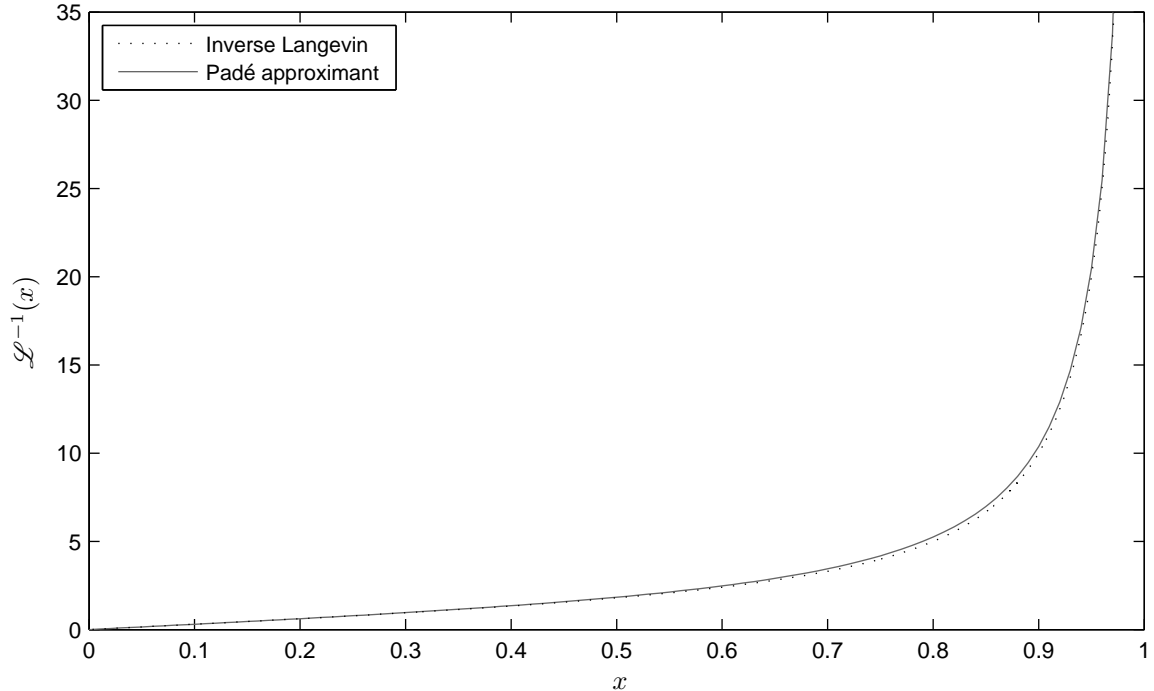


Figure 8: Comparison between the inverse Langevin function and the Padé approximant.

In our modelling of the Mullins effect we have used the Biot stress T_{B11} defined by

$$T_{B11} = \lambda^{-1}T_{11}$$

in order to facilitate comparison with experimental work.

8.1. Cyclic stress-softening for certain typical materials

Figures 9, 10, 11 and 12 depict cyclic stress-softening paths in uniaxial tension for a variety of typical materials. They have been obtained by employing variations of the following constants and functions, which have realistic values but do not correspond to any known materials:

$$N = 27.9, \quad \mu = 1.2, \quad r_1 = r_2 = 2,$$

$$A_0 = -0.115 \quad a(t) = t, \quad a_1 = 0.4,$$

$$A_{1,2}(t) = \begin{cases} -0.01 \log(0.2t) \\ -0.01 \log(0.55t) \end{cases} \quad d_\omega = \begin{cases} -0.077 \\ -0.035 \end{cases} \quad \mu b_\omega = \begin{cases} 2.38 \\ 50.0 \end{cases} \quad \vartheta_\omega = \begin{cases} 0.800 & \text{unloading,} \\ 1.000 & \text{reloading.} \end{cases}$$

In Figure 9 the Mullins effect is depicted with stress-relaxation but no residual strain or creep and so equation (16) is used for the stress. In Figure 10 we depict the Mullins effect with residual strain and the creep causing it and so use equation (22) for the stress. Figure 11 represents the Mullins effect in a material displaying stress-softening, hysteresis, stress relaxation, residual strain and creep of residual strain. This is the full model derived here and so equation

(27) is used for the stress. In Figure 12 we depict the cyclic stress softening of a carbon filled rubber vulcanizate in which the unloading proceeds to a positive stress level rather than all the way to zero. The model copes well, using the same value of W_{\max} , with this situation, which may arise in an engineering application where a rubber component, such as a spring or damper, is subject to a cyclic uniaxial tension with a continuous positive strain being applied.

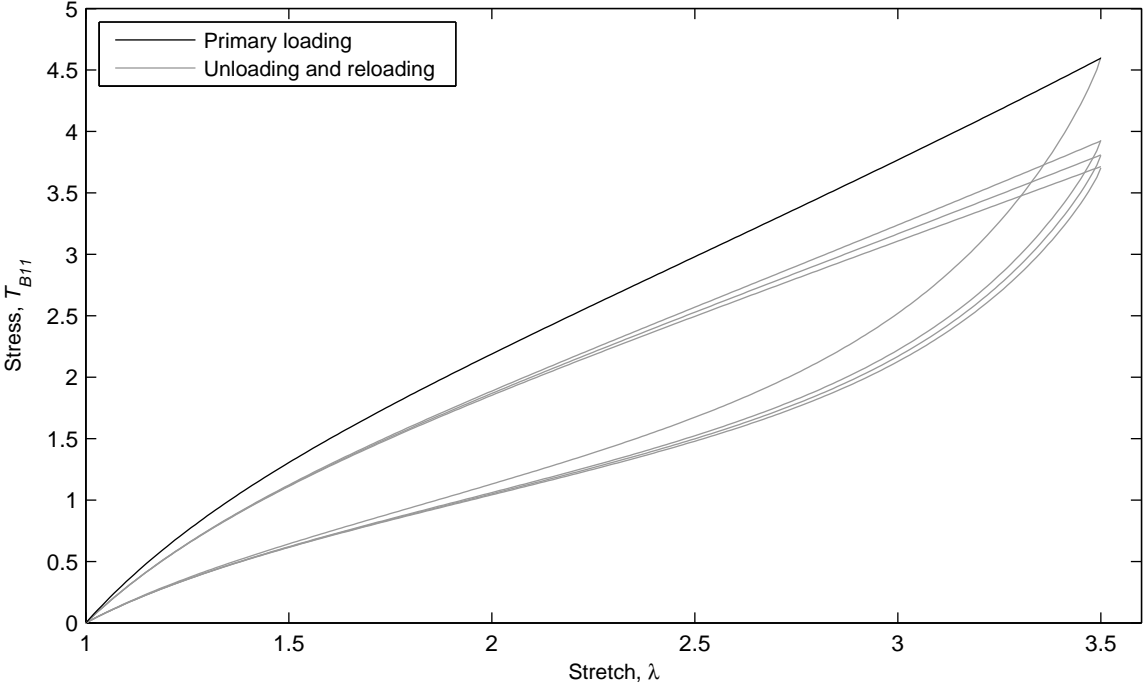


Figure 9: Cyclic stress-softening without residual strain.

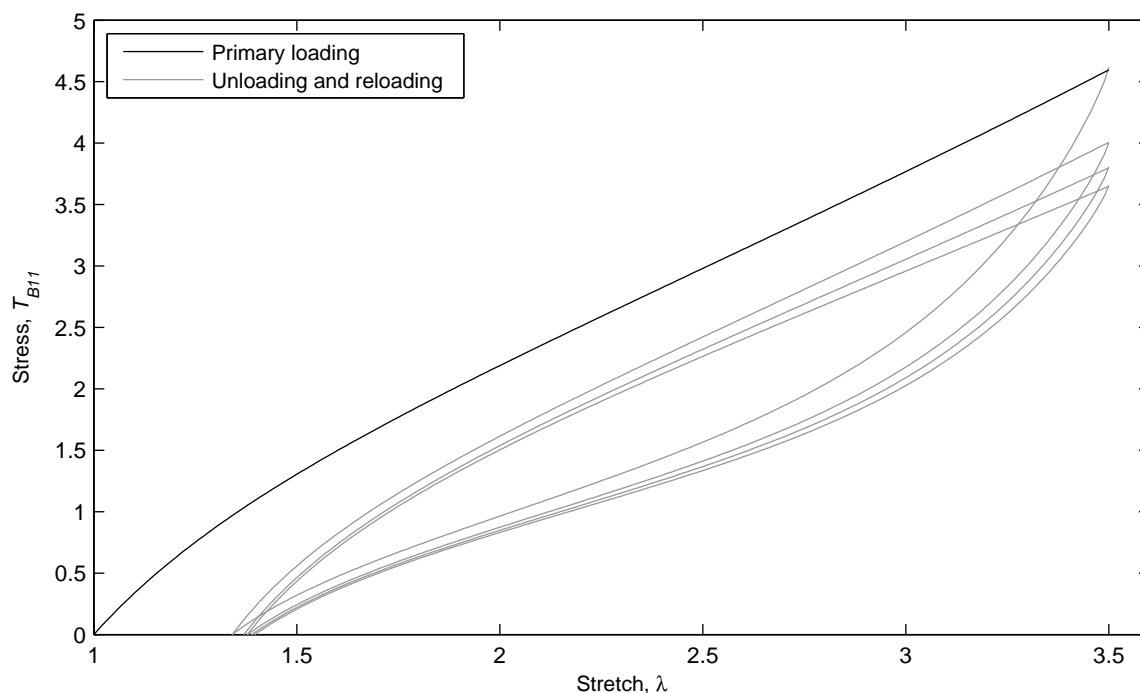


Figure 10: Cyclic stress-softening with residual strain.

8.2. Comparison with experimental data

In Figure 13 we compare the model developed here with the Arruda and Boyce (1993) model and the model of Qi and Boyce (2004). We are comparing only the first unloading path as we have been unable to identify any other model in the literature that takes into account either the first reloading path, path C of Figure 3, or further cyclic loading, see also Figure 3. In the models that have appeared in the literature the unloading/reloading paths for the cyclic process are treated as being one and the same path. We have not compared the primary loading paths as our constitutive equation, namely equation (6), for this path is the same as that presented by Arruda and Boyce (1993) and comparisons with this model have been well documented, see Zúñiga and Beatty (2002).

We see from Figure 13 that our model provides a slight improvement compared to the model of Arruda and Boyce (1993), though it should be emphasized that our model is for cyclic stress-softening. In Figures 14, 15 and 16 we provide a comparison of our constitutive model with experimental data for various concentrations of carbon-black filled natural rubber vulcanizates. This data was kindly provided by Professor A. L. Dorfmann and was presented previously by Dorfmann and Ogden (2004).

Figure 14 was obtained by using the following constants and functions in our model:

$$N = 9.3, \quad \mu = 0.375, \quad r_1 = r_2 = 1.47,$$

$$A_0 = -0.001, \quad a(t) = t, \quad a_2 = 0.4,$$

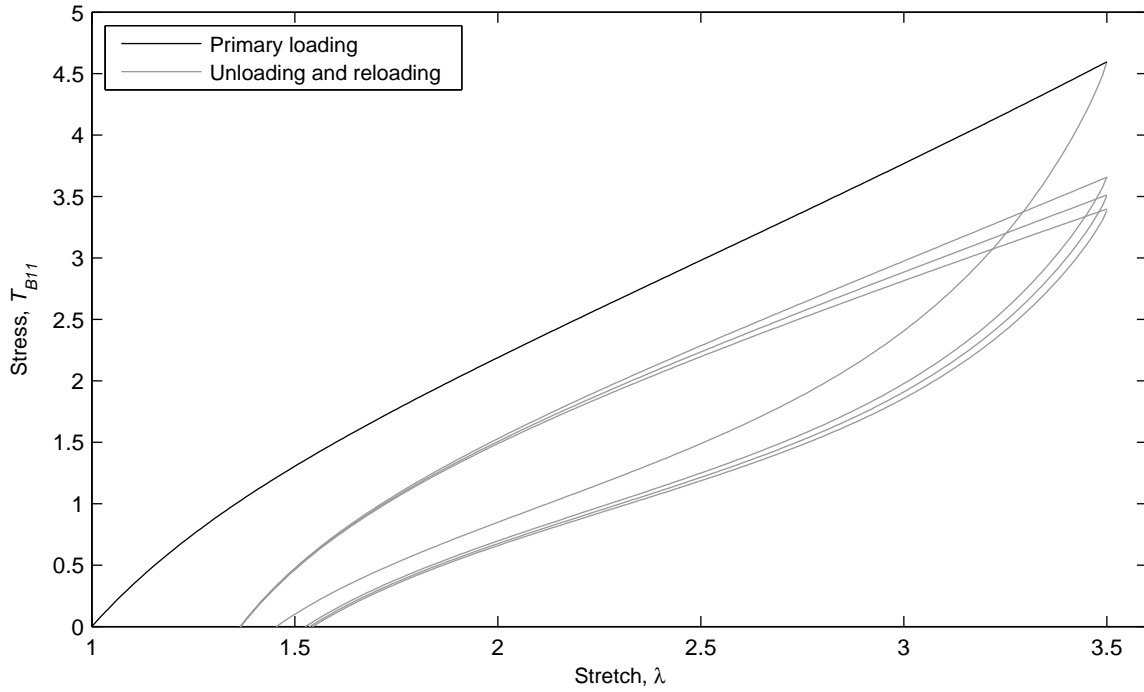


Figure 11: Cyclic stress-softening with residual strain and creep of residual strain.

$$A_{1,2}(t) = \begin{cases} -0.002 \log(0.7t) \\ -0.002 \log(1.4t) \end{cases} \quad d_\omega = \begin{cases} -0.0005 \\ -0.0003 \end{cases} \quad \mu b_\omega = \begin{cases} 28.0 \\ 28.0 \end{cases} \quad \vartheta_\omega = \begin{cases} 0.55 & \text{unloading,} \\ 0.80 & \text{reloading.} \end{cases}$$

Figure 15 was obtained by using the following constants and functions in our model:

$$N = 5.7, \quad \mu = 0.56, \quad r_1 = r_2 = 1.31,$$

$$A_0 = -0.0017, \quad a(t) = t, \quad a_2 = 1.4,$$

$$A_{1,2}(t) = \begin{cases} -0.0115 \log(0.7t) \\ -0.0115 \log(1.4t) \end{cases} \quad d_\omega = \begin{cases} -0.0014 \\ -0.0007 \end{cases} \quad \mu b_\omega = \begin{cases} 10.5 \\ 10.5 \end{cases} \quad \vartheta_\omega = \begin{cases} 0.55 & \text{unloading,} \\ 0.85 & \text{reloading.} \end{cases}$$

Figure 16 was obtained by using the following constants and functions in our model:

$$N = 5.5, \quad \mu = 1.41, \quad r_1 = r_2 = 1.11,$$

$$A_0 = -0.055, \quad a(t) = t, \quad a_2 = 0.4,$$

$$A_{1,2}(t) = \begin{cases} -0.06 \log(0.7t) \\ -0.06 \log(1.4t) \end{cases} \quad d_\omega = \begin{cases} -0.012 \\ -0.010 \end{cases} \quad \mu b_\omega = \begin{cases} 1.8 \\ 3.2 \end{cases} \quad \vartheta_\omega = \begin{cases} 0.55 & \text{unloading,} \\ 0.95 & \text{reloading.} \end{cases}$$

Figure 14 represents a specimen of rubber with a very low filler concentration, only 1phr, and the model we have developed provides an extremely accurate representation of the experimental data of Dorfmann and Ogden (2004). We observe in Figure 14 that the unloading and reloading paths are almost parallel. This is directly reflected in the choice of parameters used within the

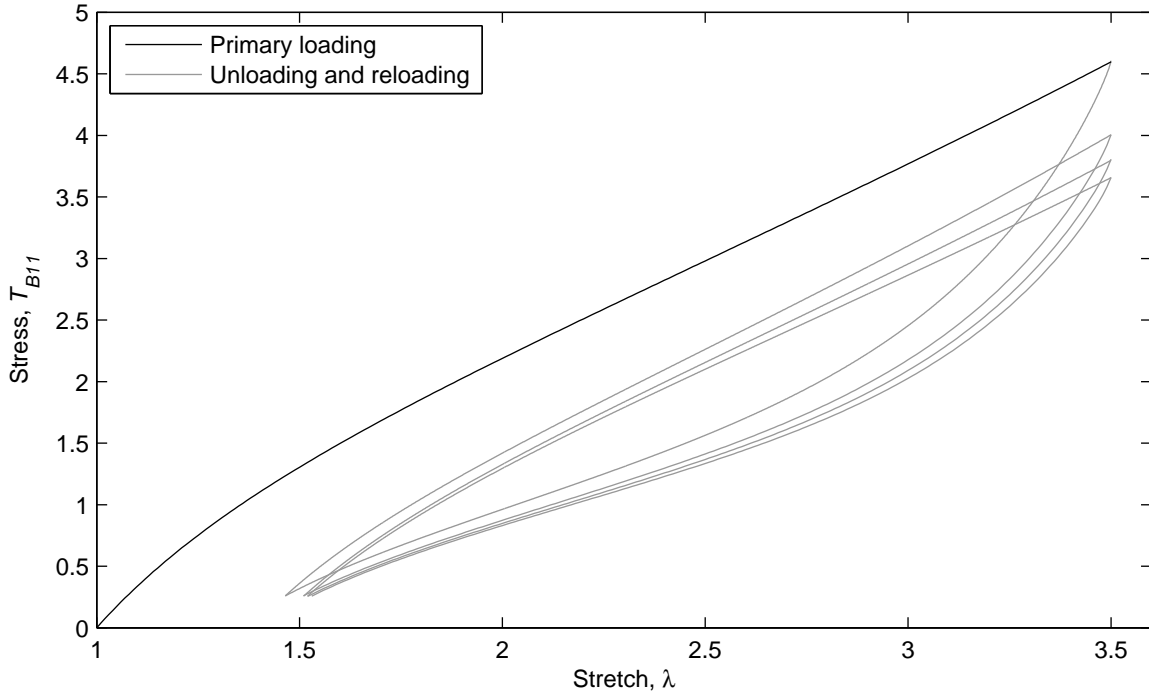


Figure 12: Cyclic stress-softening for a non-zero stress.

model, there being only a small variation in the creep parameter d_ω , see equation (26), used in unloading and reloading. There is a larger variation in the parameter ϑ_ω , see equation (10), because this is largely the parameter that governs the degree of hysteresis between the unloading and reloading paths.

The experimental data presented in Figure 15 is for a carbon filled rubber vulcanizate with an increased concentration of 20 phr but again the unloading and reloading paths are almost parallel. This is once more reflected in the choice of parameters used within the model with only ϑ_ω varying significantly between unloading and reloading.

In Figure 16 we present experimental data for a filled rubber vulcanizate with the much higher concentration of 60 phr of carbon black and observe that now the unloading and reloading paths are no longer parallel. This loss of symmetry is seen in the parameters used within the model as now d_ω and μb_ω vary between unloading and reloading, as well as ϑ_ω .

From Figures 15 and 16 we see that as the filler concentration increases the Arruda and Boyce (1993) model overestimates the stress on the primary loading path. We also observe that the accuracy of the unloading and reloading paths decreases with increased filler concentration.

9. Conclusion

The model presented here appears to be the first in which a stress-softening and residual strain model has been combined with the Arruda-Boyce eight-chain model of elasticity in order to develop a model that is capable of representing the Mullins effect for an isotropic, incompressible, hyperelastic material. Figures 9, 10 and 11 show that the model has been quite successful.

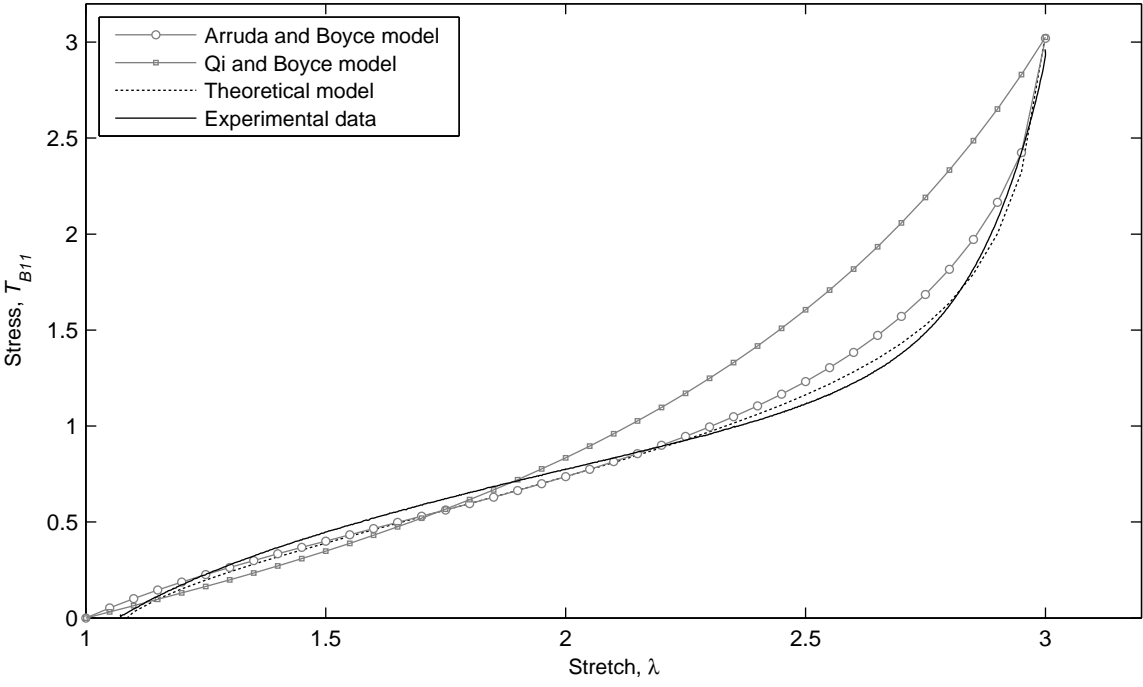


Figure 13: Comparison of the first unloading path with other constitutive models.

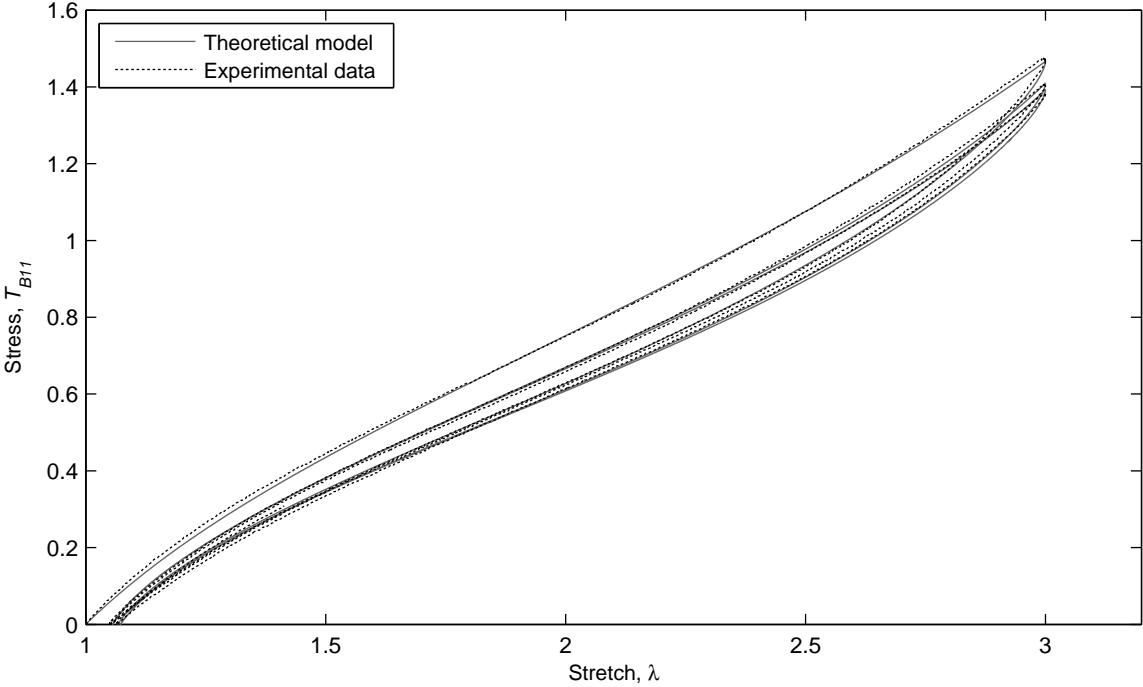


Figure 14: Comparison of our theoretical model with experimental data of Dorfmann and Ogden (2004), particle-reinforced specimen with 1 phr of carbon black.

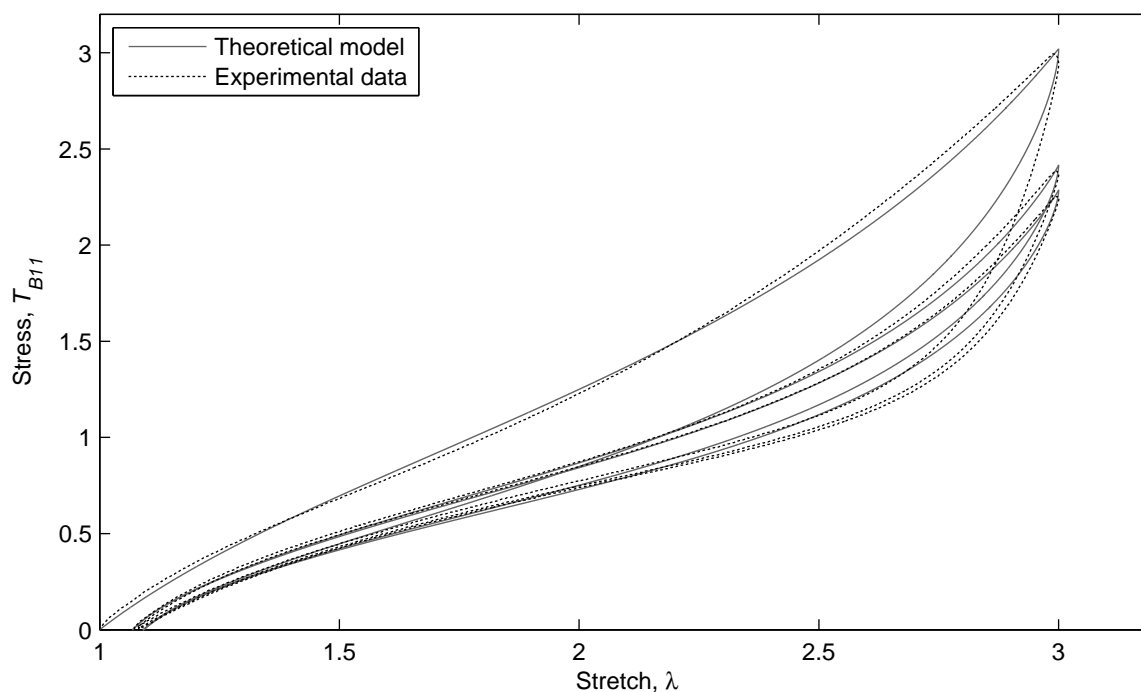


Figure 15: Comparison of our theoretical model with experimental data of Dorfmann and Ogden (2004), particle-reinforced specimen with 20 phr of carbon black.

We have considered alternative approaches to modelling the residual strain but they do not appear able to replicate the creep associated with the Mullins effect to the same degree of accuracy as the model presented here. For example, if the exponent in equation (17), and hence in the last line of equation (29), differs much from -1 then it is not possible to model the creep at all well. This argues well for the model of Bergström and Boyce (1998).

From Figure 11, we see that the model developed here provides a good representation of the Mullins effect for uniaxial tension of an isotropic rubber-like material. This model has been developed in such a way that any of the salient inelastic features can be excluded and the integrity of the model still be maintained.

We remark that Figures 15 and 16 show limited agreement with experiment though modelling correctly the broad features. This may be due to the fact that after an applied uniaxial tension the material is effectively transversely isotropic, rather than purely isotropic, because of bond-breaking and realignment. The direction of uniaxial tension would therefore become the preferred direction of transverse isotropy. We hope to present in a future paper the extension of the present model to transversely isotropic materials.

Park and Hamed (2000) and other authors have noted that unfilled vulcanized natural rubber shows negligible anisotropy as is consistent with Figure 14, which shows excellent agreement with experimental data for a very low concentration of carbon black.

The results presented here are capable of extension to equibiaxial tension and pure shear for multi-cyclic stress-strain loading. We hope to discuss these matters in a future paper.

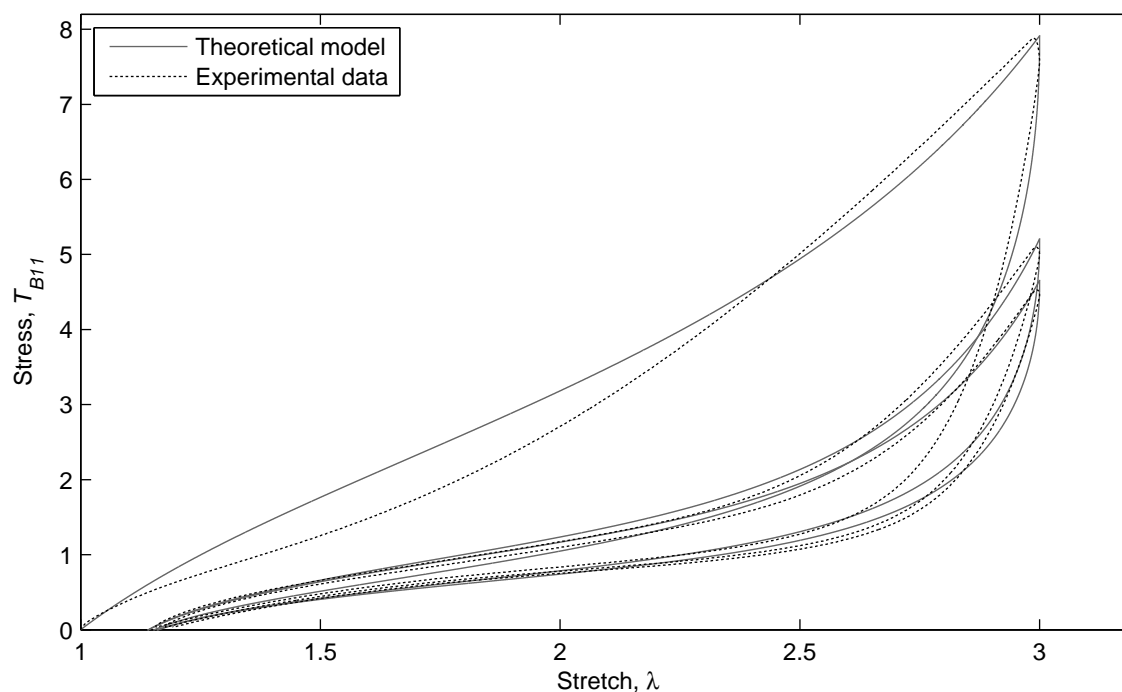


Figure 16: Comparison of our theoretical model with experimental data of Dorfmann and Ogden (2004), particle-reinforced specimen with 60 phr of carbon black.

Acknowledgements

One of us (SRR) is grateful to the University of East Anglia for the award of a PhD studentship. The authors thank Professor Luis Dorfmann for most kindly supplying experimental data. Furthermore, we would like to thank the reviewers for their constructive comments and suggestions.

References

- Arruda, E.M., Boyce, M.C., 1993. A three-dimensional constitutive model for the large stretch behavior of rubber elastic materials. *J. Mech. Phys. Solids* 41, 389–412.
- Bergström, J.S., Boyce, M.C., 1998. Constitutive modelling of the large strain time-dependent behavior of elastomers. *J. Mech. Phys. Solids* 46, 931–954.
- Bernstein, B., Kearsley, E.A., Zapas, L.J., 1963. A Study of Stress Relaxation with Finite Strain. *Trans. Soc. Rheology* VII 71, 391–410.
- Cohen, A., 1991. A Padé approximation to the inverse Langevin function. *Rheol. Acta* 30, 270–273.
- Dannenberg, E.M., 1966. Molecular slippage mechanism of reinforcement. *Trans. Inst.* 42, 26–42.

- Diani, J., Fayolle, B., Gilormini, P., 2009. A review on the Mullins effect. *Eur. Polym. J.* 45, 601–612.
- Doi, M., Edwards, S.F., 1986. *The Theory of Polymer Dynamics*. Clarendon Press, Oxford .
- Dorfmann, A., Ogden, R.W., 2003. A pseudo-elastic model for loading, partial unloading and reloading of particle-reinforced rubber. *Int. J. Solids Structures* 40, 2699–2714.
- Dorfmann, A., Ogden, R.W., 2004. A constitutive model for the Mullins effect with permanent set in particle-reinforced rubber. *Int. J. Solids Structures* 41, 1855–1878.
- Fletcher, W.P., Gent, A.N., 1953. Non-Linearity in the Dynamic Properties of Vulcanised Rubber Compounds. *Trans. Inst. Rub. Ind.* 29, 266–280.
- Holt, W.L., 1931. Behavior of rubber under repeated stresses. *Rubber Chem, Techn.* 5, 79–89.
- Johnson, M.A., Beatty, M.F., 1993. The Mullins effect in uniaxial extension and its influence on the transverse vibration of a rubber string. *Continuum Mech. Thermodyn.* 5, 83–115.
- Lockett, F.J., 1972. *Nonlinear Viscoelastic Solids*. Academic Press, London .
- Mullins, L., 1947. Effect of stretching on the properties of rubber. *J. Rubber Research* 16, 275–289.
- Ogden, R.W., Roxburgh, D.G., 1999. A pseudo-elastic model for the Mullins effect in filled rubber. *Proc. R. Soc. Lond.* 455, 2861–2877.
- Park, B., Hamed, G.R., 2000. Anisotropy in Gum and Black Filled SBR and NR Vulcanizates Due to Large Deformations. *Korea Polym. J.* 8, 268–275.
- Qi, H.J., Boyce, M.C., 2004. Constitutive model for stretch-induced softening of the stress-stretch behavior of elastomeric materials. *J. Mech. Phys. Solids* 52, 2187–2205.
- Rickaby, S.R., Scott, N.H., 2011. *The Mullins Effect. Constitutive Models for Rubber VII*, Taylor & Francis Group, London, 273–276.
- Tanner, R.I., 1988. From A to (BK)Z in constitutive relations. *J. Rheol.* 32, 673–702.
- Zúñiga, A.E., Beatty, M.F., 2002. A new phenomenological model for stress-softening in elastomers. *Z. angew. Math. Phys.* 53, 794–814.